Journal of Solid State Chemistry **142,** 325–335 (1999)
Article ID jssc.1998.8041, available online at http://www.idealibrary.com on IDEAL®

Oxygen Ionic and Electronic Transport in $LaGa_{1-x}Ni_xO_{3-\delta}$ Perovskites

A. A. Yaremchenko, V. V. Kharton,[1] A. P. Viskup, E. N. Naumovich, N. M. Lapchuk, and V. N. Tikhonovich

Institute of Physicochemical Problems, Belarus State University, 14 Leningradskaya Strasse, 220080, Minsk, Republic of Belarus

Received May 12, 1998; in revised form September 22, 1998; accepted September 23, 1998

Formation of the $LaGa_{1-x}Ni_xO_{3-\delta}$ solid solutions with perovskite structure was ascertained in the concentration range of $0 \le x \le 0.5$. Substitution of gallium with nickel results in increasing oxygen nonstoichiometry and electronic and ionic conductivities. The oxygen ion transference numbers in air at 1070–1220 K determined by the Faradaic efficiency measurements do not exceed 0.005. Oxygen permeation fluxes through $LaGa_{1-x}Ni_xO_{3-\delta}$ were found to increase with nickel content and to be limited predominantly by the bulk ionic conductivity. Reducing oxygen partial pressure leads to decreasing electronic transport and increasing ionic conductivity. Thermal expansion coefficients of the ceramics are in the range of (10.8–11.6) $\times 10^{-6}$ K^{-1}. © 1999 Academic Press

Key Words: **perovskite; mixed conductor; ionic conductivity; oxygen permeability; lanthanum gallate–nickelate.**

INTRODUCTION

Perovskite-like solid electrolytes and mixed conductors on the basis of $LaGaO_3$ are promising materials of solid oxide fuel cells (SOFCs) and ceramic membrances for oxygen separation and partial oxidation of hydrocarbons (1–10). The electrolytes of La(Sr)Ga(Mg)O_3 solid solutions possess a high oxygen ionic conductivity ($\sigma_0 > 10^{-2}$ S/cm at 870 K) with an ionic transference number $t_0 \approx 1$ over the oxygen partial pressure range of $10^{-20} < p_{O_2} < 0.4$ atm (1–6). Their advantages were reported to be a relatively low thermal expansion coefficient, close to that of yttria-stabilized zirconia (YSZ), and sufficient chemical stability (2). Testing SOFCs with anodes of nickel cermets and $La_{0.9}Sr_{0.1}Ga_{0.8}Mg_{0.2}O_{2.85}$ electrolyte demonstrated a degradation of the cells with time, caused by a solid-state interaction between the lanthanum gallate and nickel oxide forming a perovskite phase on the basis of $LaNiO_3$ (11). Studying properties of the diffusion layers between $LaGaO_3$ electrolyte and NiO is of considerable interest, because nickel-containing cermets represent a group of widely used SOFC anode materials (12).

The aim of the present work was to investigate physicochemical properties of solid solutions in the $LaGaO_3$–$LaNiO_{3-\delta}$ system, with particular emphasis on oxygen permeation processes. Our attention to this system was associated not only with studying oxygen transport through the diffusion layers in SOFCs, but also with a search for new mixed conductors for hydrocarbon oxidation reactors. Introducing cations of transition metals such as Fe, Cr, or Co into the gallium sublattice of $LaGaO_3$ was ascertained to increase regularly electronic conductivity of the solid solutions (8–10). An analogous effect could be expected when gallium is substituted with nickel. On the other hand, the substitution of gallium with nickel was expected to enlarge oxygen ion vacancy concentration, which may result in increasing ionic conductivity. Such a method for increasing oxygen transport is more preferable than incorporating strontium or barium into the lanthanum sublattice, because an interaction with water vapor accompanied with decreasing ionic conductivity is characteristic of Sr-doped $LaGaO_3$ (13). The degradation in behavior owing to the reaction with gas species like water vapor and CO_2 is typical for numerous other perovskite-like compounds containing alkaline-earth metal cations (14–17). Thus, doping lanthanum gallate by nickel was considered to be a promising strategy for increasing oxygen permeation without increasing chemical reativity of the mixed conductors.

EXPERIMENTAL

1. Synthesis and Characterization

The powders of $LaGa_{1-x}Ni_xO_{3-\delta}$ ($x = 0.2$, 0.3, 0.4, 0.5, and 0.6) were prepared by conventional solid-state reactions. The required amounts of high-purity $La(NO_3)_3 \cdot 6H_2O$, $Ni(HCOO)_2 \cdot 2H_2O$ and metallic gallium were dissolved in a nitric acid solution and then dried. After thermal decomposition of the nitrates, solid-state reactions were conducted in air at temperatures of 1630 to 1650 K for 20–35 h with multiple repeated intermediate grindings.

[1] To whom correspondence should be addressed. Fax: (375-017) 226-46-96. E-mail: kharton@fhp.bsu.unibel.by.

0022-4596/99 $30.00

Ceramic specimens were pressed into the shape of bars ($4 \times 4 \times 30$ mm) and disks of various thickness (diameter 12 or 15 mm). Gas-tight ceramics were sintered in air at 1810–1860 K during 10–20 h. After sintering, the specimens were annealed in air at 1170 K for 10–15 hours and then slowly cooled in order to obtain oxygen nonstoichiometry values as close as possible to the equilibrium ones at room temperature. The prepared ceramics were characterized using X-ray diffraction (XRD) technique, X-ray fluorescence analysis (XFA), atomic emission spectroscopy (AES), and thermal gravimetric analysis (TGA). The experimental procedures for XRD, AES, and XFA studies, TGA, EPR, testing gas tightness, and investigating electrical conductivity and thermal expansion were described in detail earlier (18–25). The oxygen nonstoichiometry values were calculated from the results of TGA studies of the powders which were reduced in a hydrogen flow at 1470–1510 K. Only specimens which had been verified to be gas tight were used for measurements of electrical conductivity, oxygen permeability, and Faradaic efficiency. The experimental technique to determine oxygen ion transference numbers by studying Faradaic efficiency was described in detail elsewhere (24, 25).

The IR spectra were recorded at room temperature on a "Spectrum-1000" Fourier transform infrared (FT-IR) instrument (produced by Perkin-Elmer). The infrared spectra were obtained in the range of 300–1200 cm^{-1} using the KBr pellet technique.

2. Oxygen Permeation Measurements

For analysis of the permeation processes, we present hereafter the oxygen flux density j ($mol \times s^{-1} \times cm^{-2}$) and specific oxygen permeability $J(O_2)$ ($mol \times s^{-1} \times cm^{-1}$). The values of $J(O_2)$ were calculated by the formula (26)

$$J(O_2) = jd \cdot \left[\ln \frac{p_2}{p_1} \right]^{-1}, \qquad [1]$$

where d is the thickness of the sample, p_2 and p_1 are the oxygen partial pressures at the membrane feed and permeate sides, respectively ($p_2 \geq p_1$).

In the case when oxygen partial pressure at the membrane permeate side is below than 0.21 atm, oxygen permeation fluxes were measured using an YSZ cell consisted of an electrochemical oxygen pump and sensor (Fig. 1A). The experimental technique was described in detail elsewhere (10, 18, 21). Oxygen permeability was determined under the condition that the oxygen flux flowing through the pump is

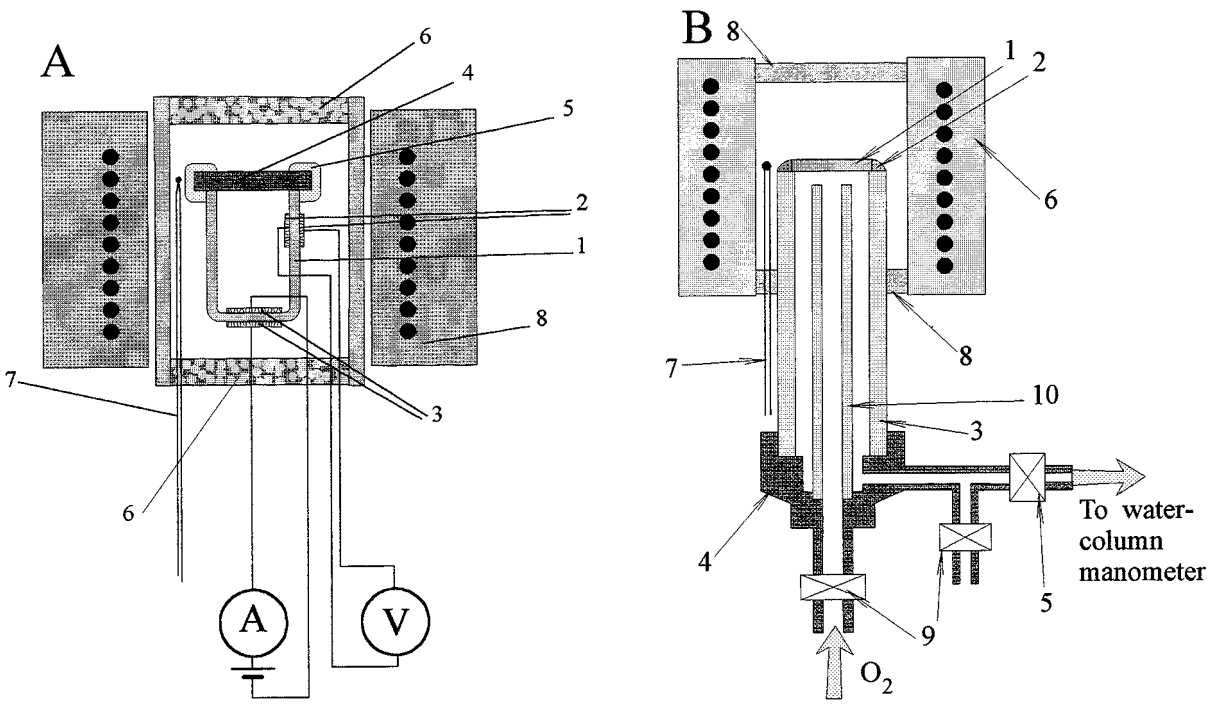

FIG. 1. Schematic drawing of the electrochemical cells for studying oxygen transport. (A) The cell for oxygen permeation measurement. 1, YSZ solid electrolyte; 2, electrodes of the oxygen sensor; 3, electrodes of the oxygen pump; 4, specimen studies; 5, high-temperature sealant; 6, high-porosity ceramic insertions; 7, thermocouple; 8, furnace. (B) The cell for oxygen permeation measurement at oxygen pressure gradient of 1.0×10^5 Pa/2.1×10^4 Pa. 1, Specimen; 2, high-temperature sealant; 3, YSZ tube; 4, metallic construction; 5, valve; 6, furnace; 7, thermocouple; 8, high-porosity ceramic insertions; 9, valves to pass oxygen through the cell before starting measurements; 10, dense alumina tube.

equal to the flux through the hermetically sealed dense membrane due to ionic transport. The values of permeation flux density and oxygen pressure at the membrane permeate side were calculated using conventional relationships

$$j = I \cdot (4FS)^{-1} \quad [2]$$

$$E = \frac{RT}{4F} \cdot \ln\left(\frac{p_2}{p_1}\right), \quad [3]$$

where I is the current passed through the oxygen pump, S is the membrane surface area, and E is the e.m.f. of the electrochemical oxygen sensor. Oxygen permeability was measured at temperatures from 960 to 1270 K. The total oxygen leakage current into the cell through the YSZ solid electrolyte and the sealants was determined separately by sealing dense YSZ disks to be less than 10 μA.

The cell shown in Fig. 1A was used mainly to investigate the permeate-side pressure dependence of the permeation flux, which corresponds to the removing of oxygen from the cell by the electrochemical pump. In this regime, p_1 was varied from 0.1 Pa to 1.5×10^4 Pa at fixed feed-side oxygen pressure ($p_2 = 2.1 \times 10^4$ Pa). Some attempts to study the dependence of oxygen permeability on the feed-side oxygen pressure were also performed using this cell. Such regime refers to pumping oxygen into the cell and to varying p_2 over the range 2.1×10^4–7.1×10^4 Pa, while maintaining p_1 equal to 2.1×10^4 Pa. However, the second regime was associated often with cracking the cell due to an excessive pumping of oxygen.

For studying permeation at oxygen partial pressure gradient of 1.0×10^5 Pa/2.1×10^4 Pa, we used a cell connected to a standard water-column manometer (Fig. 1B). Before the measurements, the specimen was sealed onto a dense YSZ tube and the cell was blown through with oxygen in order to displace atmospheric nitrogen. Then the system was isolated, which corresponds to the starting of the measurement cycle. The measured quantities were as follows: increments of pressure and volume as functions of time, atmospheric pressure, temperatures of the heated and cold parts of the device. The oxygen flux density j leaving from the cell through the specimen is defined by

$$j = S^{-1} \cdot \left[\frac{dv_0}{d\tau}\right], \quad [4]$$

where S (cm^2) is the membrane surface area, v_0 (mol) is the amount of oxygen passed out from the cell, and τ is the time after starting the measurement. The quantity v_0 as a function of time was calculated from the water-column manometer reading with consideration of the atmospheric pressure and the temperature of the system. In the measurement course, the difference of total pressures at the membrane sides was varied from 0 to 1×10^3 Pa. Under the approximation that the oxygen partial pressure gradient is constant, the time dependence of v_0 was approximated by the linear fitting model;

$$v_0 = A_1 + (jS) \cdot \tau, \quad [5]$$

where A_1 and j are the regression parameters ($A_1 \approx 0$). As a rule, the parameter A_1 which is determined by the experimental error, was statistically insignificant. The measurements were performed at temperatures 1070–1250 K with the total measurement cycle time of 25 to 100 h.

The measurement technique was verified by sealing a dense YSZ disk with *Pt* electrodes onto the cell and removing oxygen from the internal volume. In order to estimate oxygen flux determination error, the flux values calculated by Eqs. [2] and [5] were compared. Within the studied range of temperature and oxygen fluxes, the experimental error in the flux measurement was observed to not exceed 3%.

RESULTS AND DISCUSSION

1. Characterization of the Ceramics

According to the results of XRD studies, solid solutions with a rhombohedrally distorted perovskite structure form in the $LaGa_{1-x}Ni_xO_{3-\delta}$ system at $0 \le x \le 0.5$. In this composition range, all the ceramics were single phase. Their XRD patterns exhibited no additional reflections after both annealing in air and storage at room temperature for 40–50 days. As-sintered ceramics of $LaGa_{0.4}Ni_{0.6}O_{3-\delta}$ were also single phase, but a partial decomposition of the perovskite solid solution was indicated by XRD after annealing the oxide in air at temperatures above 1170 K (Fig. 2). The parameters of the rhombohedrally distorted perovskite unit cell (a and α) are listed in Table 1. Table 1 presents also the density of the ceramics (ρ_{exp}), oxygen nonstoichiometry in air (δ), and its reproducibility error, as well as TECs calculated from the dilatometric data. Doping with nickel results in increasing rhombohedral distortion of the $LaGa_{1-x}Ni_xO_{3-\delta}$ solid solution lattice and in decreasing perovskite unit cell volume. The decrease in the unit cell volume is caused by the smaller radii of Ni^{3+} cations as compared to that of Ga^{3+} (27). Thermal expansion coefficients of $LaGa_{1-x}Ni_xO_{3-\delta}$, averaged at temperatures of 300 to 1100 K, lie in the range of $(10.8–11.6) \times 10^{-6}\ K^{-1}$. Notice that TEC values of the ceramics at a low dopant content ($x \le 0.3$) are comparable with that of YSZ. Further introduction of nickel into the gallium sublattice leads to a weak increase in thermal expansion.

Oxygen vacancy concentration in $LaGa_{1-x}Ni_xO_{3-\delta}$ increases regularly with increasing nickel content and temperature (Table 1). The ratio between Ni^{2+} ion concentration and total nickel content was estimated from the oxygen

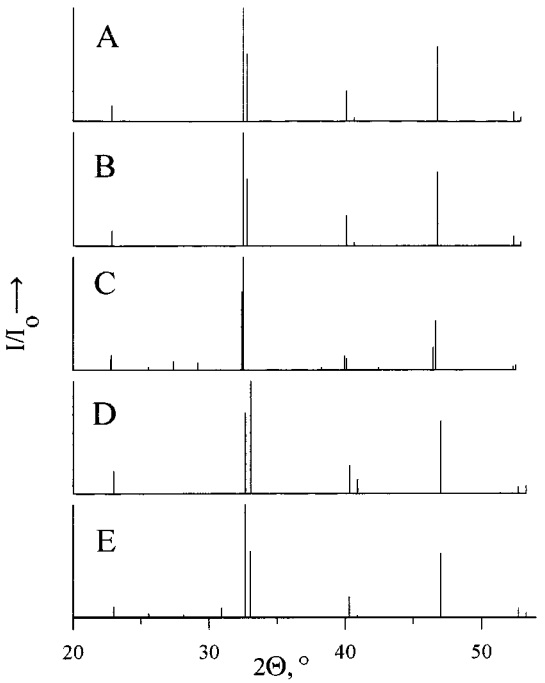

FIG. 2. Schematics of the initial fragments of XRD patterns for $LaGa_{1-x}Ni_xO_{3-\delta}$ (Cu$K\alpha$-radiation, Ni-filter): (A) $x = 0.2$ after sintering, (B) $x = 0.2$ after annealing in nitrogen at 1175 K for 75 h, (C) $x = 0.2$ after annealing in the CO–CO_2 atmosphere at 1175 K for 75 h, (D) $x = 0.6$ after sintering, (E) $x = 0.6$ after annealing in air 1270 K for 100 h.

nonstoichiometry data to be in the range of 0.27–0.42 at room temperature and 0.44–0.74 at 1130 K in air. Therewith, the fractions of divalent nickel in the $LaGa_{1-x}Ni_xO_{3-\delta}$ solid solutions at $x = 0.4$–0.6 are very close to each other—the $[Ni^{2+}]/[Ni]_{total}$ ratio is equal to 0.29–0.31 and 0.44–0.48 at room temperature and 1130 K, respectively.

Thus, substitution of gallium with nickel leads to a stabilization of Ni^{3+} oxidation state and forming perovskite-type solid solutions at nickel additions up to 50% of total *B*-site concentration. Such results are in agreement with literature data on nickel-containing perouskites. For instance, the single perovskite phase at high temperatures was reported to exist in the $LaCo_{1-x}Ni_xO_{3-\delta}$ and $(La, Sr)Mn_{1-x}Ni_xO_{3-\delta}$ systems at x values up to 0.5 ± 0.1 (28–30). The trivalent state of nickel cations in the lattice of various $LaNiO_{3-\delta}$-based perovskites was pointed out to be preferable to the divalent one (28, 31, 32).

In order to estimate a stability of the $LaGa_{1-x}Ni_xO_{3-\delta}$ solid solutions in different atmospheres, the ceramics at $x = 0.2$ were subjected to annealing in nitrogen flux ($p_{O_2} \approx 10$ Pa) and in CO–CO_2 mixture flux (about 40 vol% of CO). No appreciable changes was observed in XRD patterns of $LaGa_{0.8}Ni_{0.2}O_{3-\delta}$ after annealing in nitrogen at 1000–1200 K for 50–200 h as well as the treatment in the CO–CO_2 atmosphere at $T \leq 1070$ K. Annealing in the atmosphere containing CO at $T \geq 1170$ K was found to result in a decomposition of the solid solution phase, forming two closely related cubic perovskite phases with the unit cell parameters of 0.391 and 0.389 nm as well as unidentified phase impurities. As an example, Fig. 2 demonstrates initial fragments of the XRD patterns of $LaGa_{1-x}Ni_xO_{3-\delta}$ ceramics after annealing under various conditions.

2. *IR and EPR Spectra*

The results of IR absorption studies of $LaGa_{1-x}Ni_xO_{3-\delta}$ are presented in Fig. 3 and Table 2. All the spectra are similar, consisting of two absorption bands associated with stretching and bending vibrations. Taking into account the data on lattice vibrations of other perovskite-related oxides (33–35), a band at the higher frequency (617–622 cm^{-1}) is assigned to the stretching vibration mode of the Ga(Ni)–O bonds and that at the lower frequency (360–390 cm^{-1}) to the bending vibration. Increasing nickel content results in a split of the bending vibration band into a doublet (~ 365 and 385 cm^{-1}), related to O–Ni–O and O–Ga–O bonds, respectively. One could mention also a tendency for decreasing vibration frequency with increasing x. However, such a tendency is within the experimental error range for the materials studied.

As the resolution of the EPR spectra of $LaGa_{1-x}Ni_xO_{3-\delta}$ degrades dramatically with x, EPR signals at 77 and

TABLE 1
Properties of the $LaGa_{1-x}Ni_xO_{3-\delta}$ Ceramics

x	ρ_{exp} (kg m^{-3})	Parameters of the unit cell		Mean values of thermal expansion coefficient $\bar{\alpha} \times 10^6$, K^{-1} (300–1100 K)	Oxygen nonstoichiometry in air, δ	
		a (nm)	α (°)		300 K	1130 K
0.2	6450	0.5464	60.67	10.8 ± 0.1	0.042 ± 0.005	0.074 ± 0.001
0.3	6440	0.5461	60.66	10.8 ± 0.2		
0.4	6360	0.5451	60.71	11.6 ± 0.3	0.059 ± 0.005	0.088 ± 0.001
0.5	6380	0.5442	60.74	11.4 ± 0.3	0.068 ± 0.002	0.110 ± 0.002
0.6	6330	0.5428	60.76	11.3 ± 0.1	0.093 ± 0.001	0.145 ± 0.001

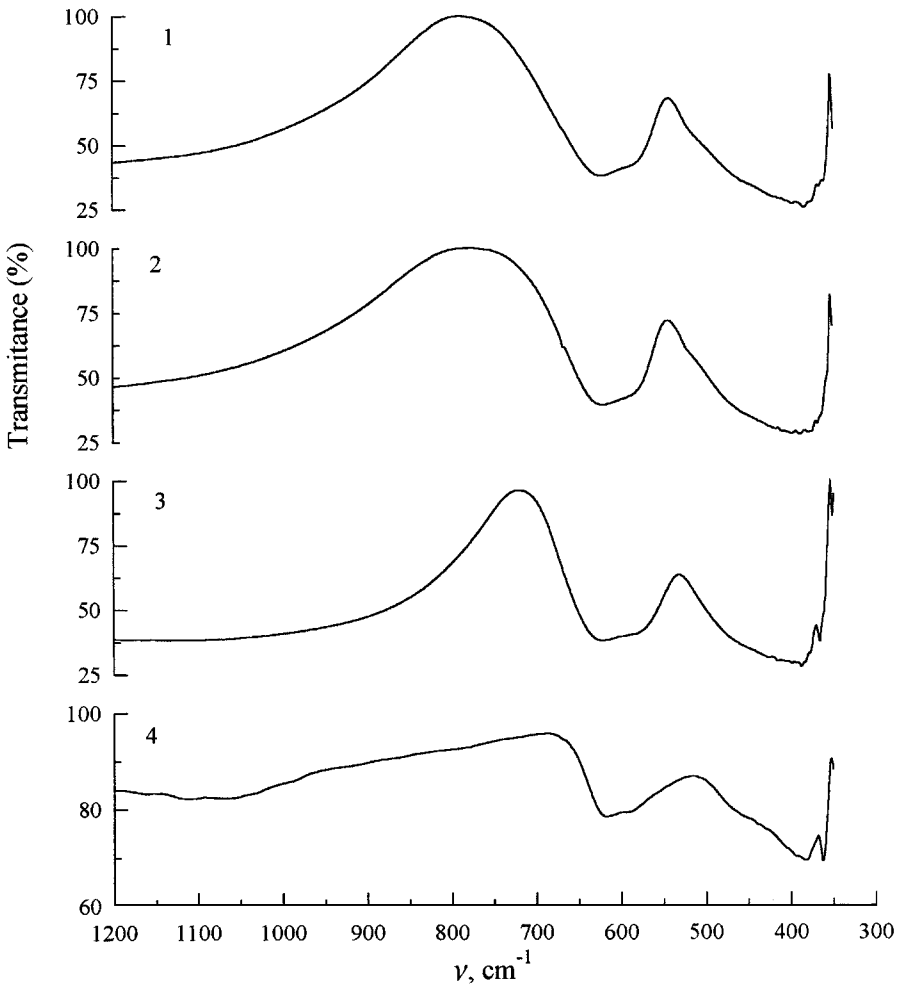

FIG. 3. IR absorption spectra of $LaGa_{1-x}Ni_xO_{3-\delta}$ at room temperature: (1) $x = 0.2$, (2) $x = 0.3$, (3) $x = 0.4$, (4) $x = 0.5$.

300 K were detectable only for the ceramics with $x = 0.2$ and 0.3 (Table 3; Fig. 4). The main reason for the poor resolution is obviously an increase in electronic conductivity of the materials with nickel additions. Another reason is assumed to be an increasing interaction of *B*-site cations with the surroundings, as discussed below.

At room temperature, the solid solutions ($x = 0.2$ and 0.3) exhibit two signals with *g*-factors of about 2.17 and 2.22.

TABLE 2
IR Absorption Bands of $LaGa_{1-x}Ni_xO_{3-\delta}$

x	ν (cm^{-1})		
0.2	622	383	—
0.3	621	389	—
0.4	622	387	365
0.5	617	383	362

The *g*-factor of the first signal agrees with that of low-spin nickel (III) in an octahedral site (36, 37). The second EPR signal is assigned to Ga^{3+} cations (10) which have a $3d^{10}$ configuration ($^1S_0$ state). The *g*-factor of ions in the *S*-state is close to that of the free electron spin (g_e) with a deviation depending on crystal field quantity. Comparing the ratio of the signal intensities to the ratio of gallium and nickel ion concentrations, one could conclude that the assignment is adequate. A weak increase of gallium ion *g*-factor with increasing *x* is assumed to be caused by a decrease in Ga–O bond ionicity (37).

Decreasing temperature from 300 to 77 K did not permit to enhance a resolution of the EPR spectra. At 77 K, two signals with closely related *g*-factors were detectable for the solid solutions with $x = 0.2$–0.3. The first of them represents a relatively narrow peak with $g = 2.169$ and 2.185 for $LaGa_{0.8}Ni_{0.2}O_{3-\delta}$ and $LaGa_{0.7}Ni_{0.3}O_{3-\delta}$, correspondingly. The second signal which refers to a broad isotropic peak ($g \approx 2.17$, $\Delta H \approx 280$ mT) is typical for all the

TABLE 3
Detectable EPR Signals of the $LaGa_{1-x}Ni_xO_{3-\delta}$ Solid Solutions

T (K)	x	g-Factor	Intensity ($A \cdot \Delta H^2/m$, relative units)	Signal width ΔH (mT)
300	0.2	2.168	48.6	20
		2.215	127.1	15
	0.3	2.165	20.5	10
		2.230	61.4	20
77	0.2	2.169	203.4	13
		2.17		280
	0.3	2.185	342.4	12
		2.17		280

Note. A is the signal amplitude; m is the specimen weight.

specimens at $x = 0.2$–0.4. Studying the EPR signal amplitude as a function of microwave field power demonstrated that the behavior of $LaGa_{1-x}Ni_xO_{3-\delta}$ is analogous to that of the La(Ga, Co)$O_{3-\delta}$ solid solutions reported earlier (10). No saturation with increasing field power was observed for $LaGa_{1-x}Ni_xO_{3-\delta}$. The spin-lattice relaxation times were estimated to be very short ($\sim 10^{-8}$ s), which can suggest a presence of broken covalent bonds (10).

In general, the results of EPR studies show that the $LaGa_{1-x}Ni_xO_{3-\delta}$ solid solutions are characterized by a more intensive interaction between B-sublattice cations than that seen in La(Ga, Co)$O_{3-\delta}$ (10). Such behavior is reflected in a poor resolution of the EPR spectra, which cannot be considered as a result of higher conductivity of nickel-doped lanthanum gallate only. Indeed, a relative insulated state of cobalt cations with respect to the interaction with the surroundings was ascertained for La(Ga, Co)$O_{3-\delta}$ perovskites (10), whereas EPR behavior of the La(Ga, Co, Mg)$O_{3-\delta}$ solid solutions is similar to that of $LaGa_{1-x}Ni_xO_{3-\delta}$ (38). A comparison between the results of the present work and EPR data on La(Ga, Co)$O_{3-\delta}$ (10) and La(Ga, Co, Mg)$O_{3-\delta}$ (38) leads us to an assumption that increasing interaction of B cations with surroundings is a direct consequence of an increase in oxygen vacancy concentration.

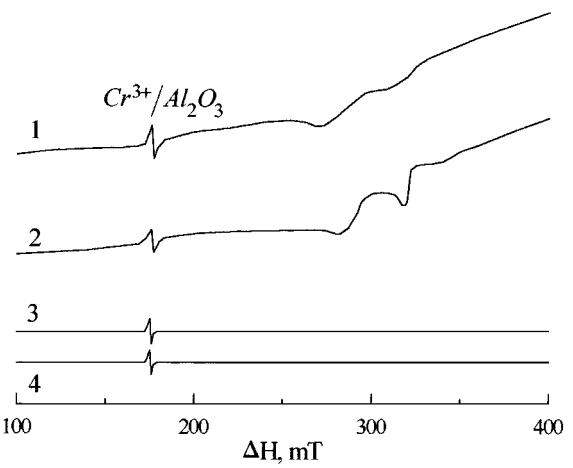

FIG. 4. EPR spectra of $LaGa_{1-x}Ni_xO_{3-\delta}$ at room temperature: (1) $x = 0.2$, (2) $x = 0.3$, (3) $x = 0.4$, (4) $x = 0.5$.

3. *Electrical Conductivity*

The substitution of gallium with nickel results regularly in increasing electrical conductivity of $LaGa_{1-x}Ni_xO_{3-\delta}$ (Fig. 5). Therewith, a metallic conductivity is characteristic of the $LaGa_{0.4}Ni_{0.6}O_{3-\delta}$ ceramics within all the temperature range studied, and the solid solutions with $x = 0.4$ and 0.5 exhibit a metal–insulator transition at temperatures above 1000 K. Similar to the La(Ga, M)O_3 (M = Fe, Cr, or Co) systems (8–10), increasing electronic conductivity with x seems to be reasonably expected. Electronic conduction in ABO_3 perovskites occurs via B–O–B bonds and is primarily dependent on their delocalization (39). Lanthanum nickelate $LaNiO_{3-\delta}$ is known to behave as a semimetal within a wide temperature range, which can be interpreted in terms of a conduction band formed by the hybridization of p-orbitals of oxygen and e_g-orbitals of low-spin trivalent nickel ions (40, 41). Increasing gallium concentration in the $LaGa_{1-x}Ni_xO_{3-\delta}$ solid solutions results in progressive localization of the atomic levels as well as decreasing bandwidth. This is attributed to increasing activation energy for

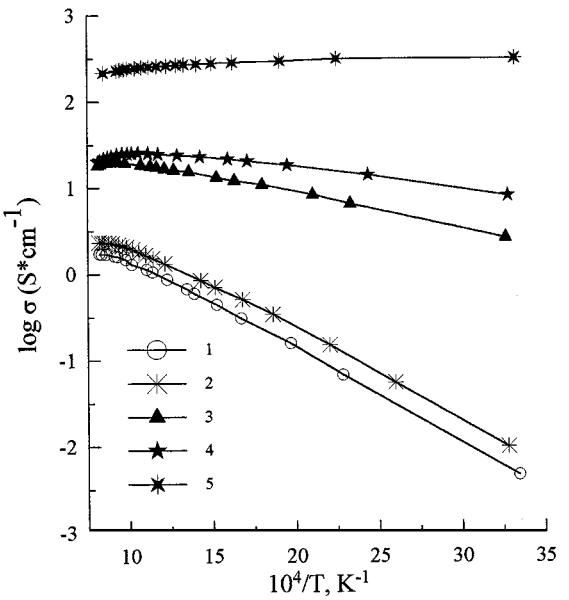

FIG. 5. Temperature dependence of the electrical conductivity of the $LaGa_{1-x}Ni_xO_{3-\delta}$ ceramics in air: (1) $x = 0.2$, (2) $x = 0.3$, (3) $x = 0.4$, (4) $x = 0.5$, (5) $x = 0.6$.

TABLE 4
Regression Parameters of the Temperature Dependence of the Electrical Conductivity of $LaGa_{1-x}Ni_xO_{3-\delta}$ Ceramics in Air

x	T (K)	E_a (kJ mol^{-1})	$\ln(A_0)$ (S × cm^{-1})	ρ
0.2	300–1150	24.6 ± 0.2	10.18 ± 0.03	0.9999
0.3	300–1150	23.5 ± 0.2	10.42 ± 0.03	0.9999
0.4	300–1020	11.7 ± 0.2	11.24 ± 0.03	0.9997
0.5	300–950	8.5 ± 0.1	11.14 ± 0.02	0.9999

Note. ρ is the correlation coefficient of the model Eq. [6].

electrical conductivity (Table 4). The activation energy was calculated by the standard Arrhenius model

$$\sigma = \frac{A_0}{T} \cdot \exp\left[-\frac{E_a}{RT} \right], \qquad [6]$$

where σ is the specific electrical conductivity, A_0 is the preexponential factor, and E_a is the activation energy. Table 4 lists the regression parameters obtained by fitting of the experimental data, including the correlation coefficient (ρ) of the model Eq. [6]. Increasing gallium content from 50 to 80% of B sites leads to increasing activation energy from 8.5 to 24.6 kJ/mol. The E_a values at high gallium concentrations ($x = 0.2$–0.3) are close to each other, indicating that the conduction mechanism is the same. Most probably, electronic transport in this case occurs via carrier hopping between nickel cations.

Reducing oxygen partial pressure was observed to decrease conductivity of $LaGa_{1-x}Ni_xO_{3-\delta}$ (Fig. 6). This is caused by leaving oxygen from the perovskite crystal lattice and decreasing trivalent nickel cation concentration. Such behavior can suggest p-type electronic conduction (42).

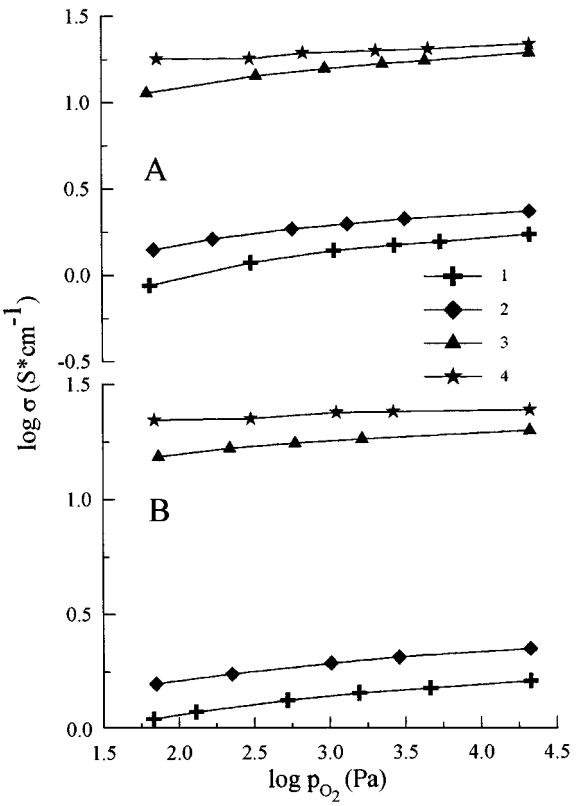

FIG. 6. Dependence of the electrical conductivity of the $LaGa_{1-x}Ni_xO_{3-\delta}$ ceramics on the oxygen partial pressure at 1173 ± 3 K (A) and 1073 ± 3 K (B): (1) $x = 0.2$, (2) $x = 0.3$, (3) $x = 0.4$, (4) $x = 0.5$.

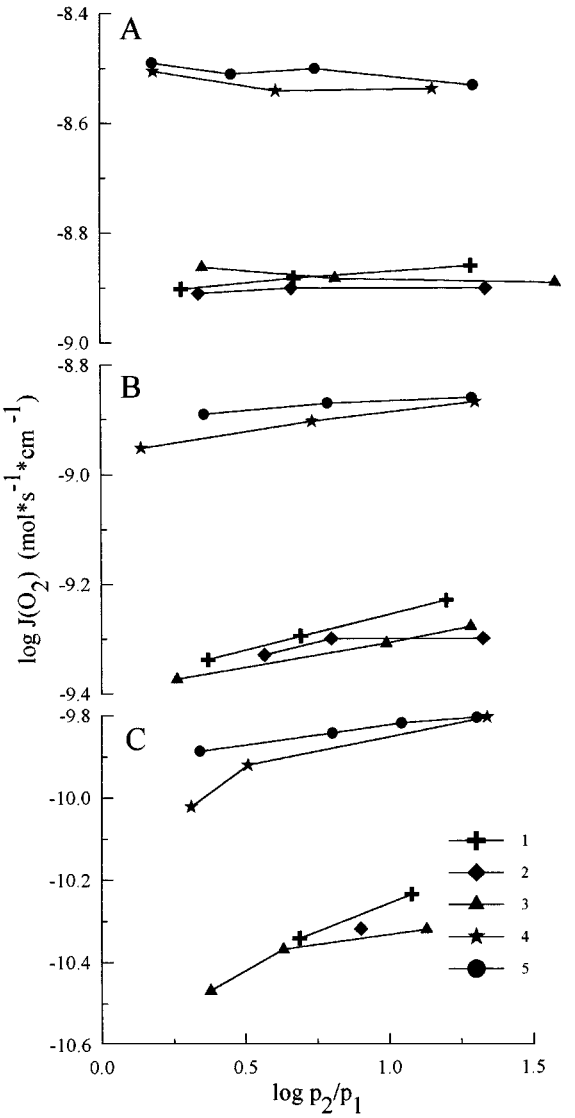

FIG. 7. Dependence of oxygen permeability of the $LaGa_{1-x}Ni_xO_{3-\delta}$ ceramics on the oxygen partial pressure differential ($p_2 = 2.1 \times 10^4$ Pa) at 1223 ± 3 K (A), 1173 ± 3 K (B), and 1073 ± 3 K (C): (1) $x = 0.2$, $d = 1.00$ mm; (2) $x = 0.2$, $d = 0.58$ mm; (3) $x = 0.2$, $d = 1.00$ mm, membrane with porous Pt layers; (4) $x = 0.4$, $d = 1.00$ mm; (5) $x = 0.4$, $d = 0.60$ mm.

However, our attempts to fit the experimental data using conventional models of power dependence of the electrical conductivity on oxygen pressure (42) showed that the power models are not adequate in the case of $LaGa_{1-x}Ni_xO_{3-\delta}$. Thus, further investigations are required in order to refine electronic transport mechanism in the perovskites studied.

4. Oxygen Ionic Transport

Figure 7 presents the dependence of specific oxygen permeability for the $LaGa_{1-x}Ni_xO_{3-\delta}$ membranes of different thickness on the permeate-side oxygen pressure. For the membranes of various thickness, the variation in the oxygen permeability values was within the reproducibility error range (about 15%). Observed regularity indicates that an effect of oxygen exchange rates at the membrane/gas boundaries on the permeation fluxes is insignificant. Indeed, $J(O_2)$ values were calculated to be proportional to $j \times d$ (see Eq. [1]). In case the permeation flux is not affected by the interphase exchange rates, one can expect $J(O_2)$ to be independent of membrane thickness. Otherwise, $J(O_2)$ should increase with increasing d due to the reducing role of the surface limitation at a given oxygen chemical potential gradient (21). Thus, the limiting factor of the oxygen transport through $LaGa_{1-x}Ni_xO_{3-\delta}$ ceramics at the membrane thickness above 0.5 mm is the bulk ambipolar conductivity, which represents a function of partial ionic and electronic conductivities.

Oxygen ion transference numbers determined by the Faradaic efficiency measurements are adduced in Table 5. At 1075–1225 K, the ion transference numbers of the solid solutions with $x = 0.2$ and 0.3 lie in the range from 4×10^{-4} to 5×10^{-3}. An increase of the transference numbers with temperature suggests that the activation energy for ionic conductivity is higher than that of electronic conductivity. Increasing nickel content results in increasing ionic conductivity of the materials due to increasing oxygen vacancy concentration. For the ceramics with $x > 0.3$, the direct measurement of the transference numbers was impossible because the electronic conductivity is much higher in comparison with ionic conductivity. Taking into consideration the results of Faradaic efficiency and oxygen permeability studies, one can conclude that oxygen permeation fluxes through $LaGa_{1-x}Ni_xO_{3-\delta}$ are limited predominantly by the ionic conductivity of the perovskites.

This conclusion was confirmed by calculations of the ion transference numbers from the permeation data using the formula (26)

$$J(O_2) = \frac{RT}{16F^2} \cdot t_o(1 - t_o) \cdot \sigma, \qquad [7]$$

where σ is the specific electrical conductivity. Generally, Eq. [7] is oversimplified and can be applied only in case when there are no surface limitations of the permeation flux and both ionic and electronic conductivities are independent of oxygen pressure. Table 5 lists the ion transference numbers calculated by Eq. [7] from the data on conductivity and oxygen permeation at "oxygen/atmospheric air" gradients. The values of t_0, estimated by this method, are quite close to ones determined by the Faradaic efficiency measurements. This substantiates our conclusion about ionic conductivity as the permeation-determining factor.

The substitution of gallium with nickel was established to lead to an increase in both ionic conductivity and oxygen

TABLE 5
Oxygen Ion Transference Numbers of the $LaGa_{1-x}Ni_xO_{3-\delta}$ Ceramics

		Transference number determined by the Faradaic efficiency measurements[a]			Transference numbers calculated from the oxygen permeation data[b]	
x	T (K) ($\pm$ 3 K)	t_0	ρ_1	σ_0	t_0	ρ_2
0.2	1073	0.0006 ± 0.0002	0.9557	9.6×10^{-4}	0.0005	0.9964
	1173	0.0011 ± 0.0001	0.9994	1.9×10^{-3}	0.0010	0.9961
	1223	0.0026 ± 0.0001	0.9998	4.5×10^{-3}	0.0022	0.9996
0.3	1073	0.0004 ± 0.0001	0.9840	8.9×10^{-4}	0.0004	0.9950
	1173	0.0030 ± 0.0001	0.9996	7.0×10^{-3}	0.0012	0.9982
	1223	0.0049 ± 0.0001	0.9998	1.1×10^{-2}	0.0027	0.9997

Note. σ_0 is the oxygen ionic conductivity calculated from the data of Faradaic efficiency and total conductivity. ρ_2 is the correlation coefficient of the regression model Eq. [5].

[a] The ion transference numbers were determined at negligible oxygen chemical potential gradient.

[b] The transference numbers were calculated by Eq. [7] from the data on conductivity and oxygen permeability. The permeation data refers to the specimens with applied Pt-layers, thickness of 1.00 mm and oxygen pressure gradient of 1.0×10^5 Pa/2.1×10^4 Pa.

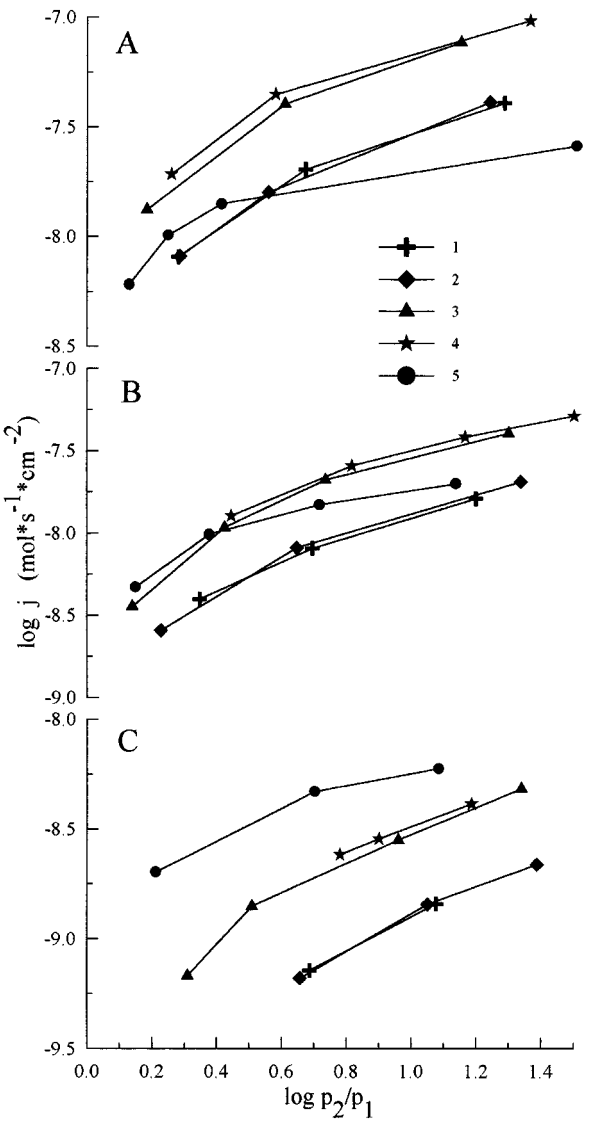

FIG. 8. Dependence of oxygen permeation flux density through $LaGa_{1-x}Ni_xO_{3-\delta}$ ceramics on the oxygen partial pressure differential at fixed feed-side pressure ($p_2 = 2.1 \times 10^4$ Pa) and $T = 1223 \pm 3$ K (A), 1173 ± 3 K (B), and 1073 ± 3 K (C). Thickness of the membranes is 1.00 ± 0.01 mm: (1) $x = 0.2$, (2) $x = 0.3$, (3) $x = 0.4$, (4) $x = 0.5$, (5) $x = 0.6$. The data for $LaGa_{0.4}Ni_{0.6}O_{3-\delta}$ corresponds to the starting period of the measurement cycle before degradation process (see text).

permeation fluxes owing to increasing oxygen vacancy concentration (Fig. 8). Here, one can recognize two groups of the $LaGa_{1-x}Ni_xO_{3-\delta}$ ceramics: at $x = 0.2$–0.3 and at $x = 0.4$–0.5. The permeability values within each of these two groups are very close. Similar dependences on composition of the solid solutions are typical also for total electrical conductivity (Fig. 5) and EPR spectra (Fig. 4). More detailed studies are necessary to clarify its nature. The permeation fluxes through $LaGa_{0.4}Ni_{0.6}O_{3-\delta}$ membranes at $T \geq 1170$ K were found to be less than ones of $LaGa_{0.5}Ni_{0.5}O_{3-\delta}$. In addition, the ceramics of $LaGa_{0.4}Ni_{0.6}O_{3-\delta}$ exhibited a degradation of the permeation fluxes with time. While oxygen permeability of this material was approximately constant after steady-state attainment during first 80–100 h of the measurement cycle, further tests under fixed oxygen pressure gradient resulted in a decrease of the permeation flux by a factor of 3–10. Obviously, the reason for the degradation in behavior is the phase decomposition of the $LaGa_{0.4}Ni_{0.6}O_{3-\delta}$ ceramics with time (Fig. 2). No degradation was found for other ceramic materials.

Analogously to incorporation of nickel into the gallium sublattice, decreasing oxygen partial pressure leads to an increase in oxygen vacancy concentration and oxygen permeability (Figs. 9 and 10). The slope of temperature dependences of the permeation fluxes is approximately constant for each material, being independent of oxygen pressure gradient. Such behavior suggests that oxygen ion migration energy does not depend on ion charge carrier concentration. Depositing porous platinum layers with the sheet density of approximately $10\ \text{mg} \times \text{cm}^{-2}$ onto membrane surfaces exhibits no effect on the oxygen permeability (Figs. 7 and 10), which attests oxygen ionic conduction to be flux-limiting factor.

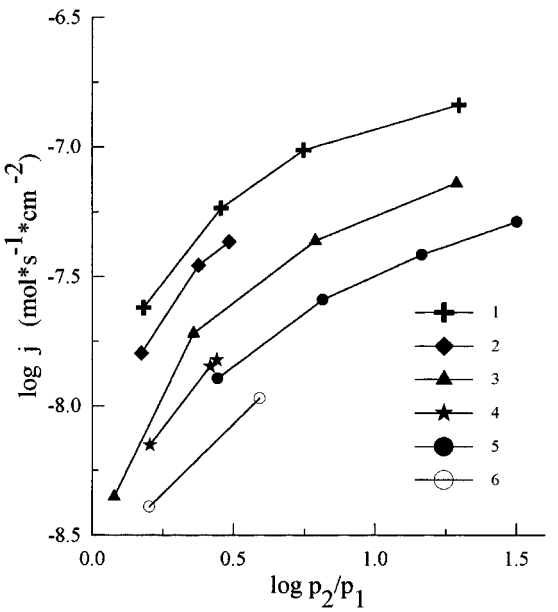

FIG. 9. Dependence of oxygen permeation flux density through $LaGa_{1-x}Ni_xO_{3-\delta}$ ceramics on the oxygen partial pressure differential. Curves 1, 3, and 5 correspond to the permeate-side oxygen pressure dependence of the flux at fixed feed-side pressure ($p_2 = 2.1 \times 10^4$ Pa). Curves 2, 4, and 6 relate to the feed-side pressure dependence for the same membranes at fixed permeate-side pressure ($p_1 = 2.1 \times 10^4$ Pa). 1 and 2, $x = 0.4$, 1223 K, $d = 0.60$ mm; 3 and 4, $x = 0.4$, 1173 K, $d = 0.60$ mm; 5 and 6, $x = 0.5$, 1173 K, $d = 1.00$ mm.

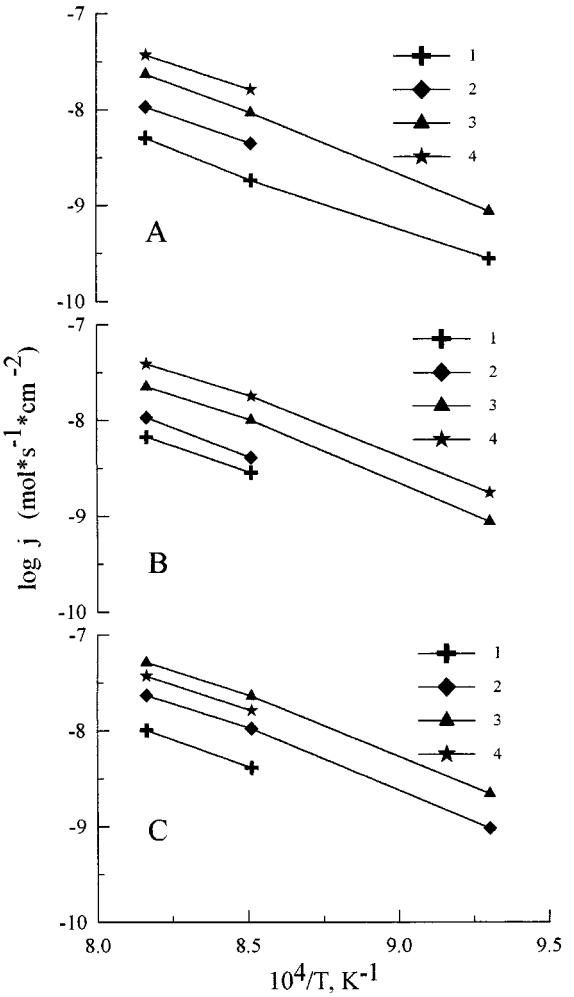

FIG. 10. Temperature dependence of the permeation flux density through $LaGa_{1-x}Ni_xO_{3-\delta}$ ceramics at fixed oxygen partial pressures: (1) $p_1 = 2.1 \times 10^4$ Pa, $p_2 = 1.0 \times 10^5$ Pa; (2) $p_1 = 8.4 \times 10^3$ Pa, $p_2 = 2.1 \times 10^4$ Pa; (3) $p_1 = 3.3 \times 10^3$ Pa, $p_2 = 2.1 \times 10^4$ Pa; (4) $p_1 = 1.3 \times 10^3$ Pa, $p_2 = 2.1 \times 10^4$ Pa. Thickness of the membranes is 1.00 ± 0.01 mm. (A) $x = 0.2$; (B) $x = 0.3$ (curve 1 corresponds to the membrane with deposited porous Pt layers); (C) $x = 0.4$ (curve 1 corresponds to the membrane with Pt layers).

CONCLUSIONS

1. Formation of solid solutions with rhombohedrally distorted perovskite structure was found in the $LaGa_{1-x}Ni_xO_{3-\delta}$ ($0 \le x \le 0.5$) system. Substitution of gallium with nickel results in increasing thermal expansion and oxygen nonstoichiometry. Thermal expansion coefficients of the ceramics are in the range of $(10.8–11.6) \times 10^{-6}$ K^{-1}. The perovskite-type unit cell volume decreases with nickel additions.

2. Electronic conductivity of the $LaGa_{1-x}Ni_xO_{3-\delta}$ ($x =$ 0.2–0.6) was ascertained to dominate over ionic conductivity. The oxygen ion transference numbers at 1070–1220 K were determined by the Faradaic efficiency measurements and do not exceed 0.005. Electronic conductivity of the ceramics increases with nickel content and decreases with reducing oxygen partial pressure. The activation energy for electronic conduction was calculated to decrease from 24.6 to 8.6 kJ/mol when x increases in the range 0.2–0.5.

3. Oxygen permeation fluxes through $LaGa_{1-x}Ni_xO_{3-\delta}$ at the membrane thickness above 0.5 mm were demonstrated to be limited by the bulk ionic conductivity of the materials. Decreasing oxygen pressure leads to increasing ionic conductivity and oxygen permeability of the solid solutions, caused by increasing oxygen ion vacancy concentration. Increasing nickel content was observed to exhibit similar effect on the ion transport properties.

ACKNOWLEDGMENTS

This work was partially supported by the Belarus Foundation for Basic Research, by the Belarus Ministry of Education and Science, and by the company B-2 Ltd. The authors are sincerely grateful to the Department of Custom Examination and Analysis of the Minsk Regional Custom for IR spectra measurements.

REFERENCES

1. T. Ishihara, H. Matsuda, and Y. Takita, *J. Am. Chem. Soc.* **116,** 3801 (1994).
2. M. Feng and J. B. Goodenough, *Eur. J. Solid State Inorg. Chem.* **31,** 663 (1994).
3. T. Ishihara, H. Matsuda, and Y. Takita, *Solid State Ionics* **79,** 147 (1995).
4. P. Huang and A. Petric, *J. Electrochem. Soc.* **143,** 1644 (1996).
5. J. W. Stevenson, T. R. Armstrong, D. E. McGready, L. R. Pederson, and W. J. Weber, *J. Electrochem. Soc.* **144,** 3613 (1997).
6. J. Drennan, V. Zelizko, D. Hay, F. T. Ciacci, S. Rajendran, and S. P. Badwal, *J. Mater. Chem.* **7,** 79 (1997).
7. K. Nomura and S. Tanase, *Solid State Ionics* **98,** 229 (1997).
8. M. Schwartz, J. H. White, and A. F. Sammells, International Patent Application PCT WO 97/41060 (1997).
9. T. R. Baker, B. Gharbage, and F. M. Marques, *J. Electrochem. Soc.* **144,** 3130 (1997).
10. V. V. Kharton, A. P. Viskup, E. N. Naumovich, and N. M. Lapchuk, *Solid State Ionics* **104,** 67 (1997).
11. K. Huang, M. Feng, J. B. Goodenough, and C. Milliken, *J. Electrochem. Soc.* **144,** 3620 (1997).
12. K. Kinoshita, "Electrochemical Oxygen Technology." Wiley-Interscience, New York-Chichester-Brisbane-Toronto-Singapore, 1992.
13. B. Gharbage, T. R. Baker, and F. M. Marques, *J. Mater. Sci. Lett.* **17,** 75 (1998).
14. M. F. Carolan, P. N. Dyer. J. M. LaBar, Thorogood, U.S. Patent 5,240,473 (1993).
15. M. F. Carolan, P. N. Dyer, S. M. Fine, J. M. LaBar, R. M. Thorogood, U. S. Patent 5,269,822 (1993).
16. S. Pei, M. S. Kleefisch, T. P. Kobylinsky, J. Faber, C. A. Udovich, V. Zhang-McCoy, B. Dabrowski, U. Balachandran, R. L. Mieville, and R. B. Poeppel, *Catal. Lett.* **30,** 201 (1995).
17. A. Manthiram, J. F. Kuo, and J. B. Goodenough, *Solid State Ionics* **62,** 225 (1993).

18. V. V. Kharton, E. N. Naumovich, A. A. Vecher, and A. V. Nikolaev, *J. Solid State Chem.* **120,** 128 (1995).
19. V. V. Kharton, A. V. Nikolaev, E. N. Naumovich, and A. A. Vecher, *Solid State Ionics* **81,** 201 (1995).
20. A. V. Kovalevsky, V. V. Kharton, and E. N. Naumovich, *Inorg. Mater.* **32,** 1230 (1996).
21. V. V. Kharton, Li Shuangbao, A. V. Kovalevsky, and E. N. Naumovich, *Solid State Ionics* **96,** 141 (1997).
22. V. V. Kharton, E. N. Naumovich, and V. V. Samokhval, *Solid State Ionics* **99,** 269 (1997).
23. E. N. Naumovich, S. A. Skilkov, V. V. Kharton, A. A. Tonoyan, and A. A. Vecher, *Russ. J. Electrochem.* **30,** 642 (1994).
24. A. A. Yaremchenko, V. V. Kharton, E. N. Naumovich, A. A. Tonoyan, and V. V. Samokhval, *J. Solid State Electrochem.* **2,** 308 (1998).
25. A. A. Yaremchenko, V. V. Kharton, E. N. Naumovich, and V. V. Samokhval, *Solid State Ionics* **111,** 227 (1988).
26. H.-H. Moebius, Extend. Abstr. 37th Meet. ISE (Vilnius, USSR, 1986), Vol. 1, p. 136.
27. R. D. Shannon and C. T. Prewitt, *Acta Crystallogr. B* **25,** 925 (1969).
28. I. F. Kononyuk, N. G. Surmach, S. P. Tolochko, and T. V. Kugan, *Neorg. Mater.* **20,** 1203 (1984). [in Russian]
29. M. Hrovat, N. Katsarakis, K. Reichmann, S. Bernik, D. Kuscer, and J. Holc, *Solid State Ionics* **83,** 99 (1996).
30. Yu. S. Gaiduk, V. V. Kharton, E. N. Naumovich, and V. V. Samokhval, *Inorg. Mater.* **30,** 759 (1994).
31. I. Alvarez, M. L. Veiga, and C. Pico, *Solid State Ionics* **91,** 265 (1996).
32. H. E. Hoefer and W. F. Kock, *J. Electrochem. Soc.* **140,** 2889 (1993).
33. G. V. Subba Rao, C. N. R. Rao, and J. R. Ferraro, *Appl. Spectrosc.* **24,** 436 (1970).
34. P. Ganguly and C. N. R. Rao, *J. Solid State Chem.* **53,** 193 (1984).
35. Y. Y. Kim, D. H. Lee, T. Y. Kwon and S. H. Park, *J. Solid State Chem.* **112,** 376 (1994).
36. G. Demazeau, J. L. Marty, M. Pouchard, T. Rojo, J. M. Dance, and P. Hagenmuller, *Mater. Res. Bull.* **16,** 47 (1981).
37. G. Demazeau, S.-H. Byeon, J. M. Dance, J.-H. Choy, M. Pouchard, and P. Hagenmuller, *Eur. J. Solid State Inorg. Chem.* **29,** 283 (1992).
38. A. A. Yaremchenko, V. V. Kharton, A. P. Viskup, E. N. Naumovich, and N. M. Lapchuk, *Solid State Ionics*, in press.
39. N. Ramadass, *Mater. Sci. Eng.* **36,** 231 (1978).
40. K. P. Rajeev, G. V. Shivashankar, and A. K. Raychaudhuru, *Solid State Commun.* **79,** 591 (1991).
41. M. Medarde, A. Fontaine, J. L. Garcia-Munoz, J. Rodriguez-Carvajal, M. de Santis, M. Sacchi, G. Rossi, and P. Lacorre, *Phys. Rev. B* **46,** 14975 (1992).
42. P. Kofstad "Nonstoichiometry, Diffusion and Electrical Conductivity in Binary Metal Oxides." Wiley-Interscience, New York, 1972.